Underactuated Robotic Fish Control: Maneuverability and Adaptability through Proprioceptive Feedback*

Gianluca Manduca[1,2][0000−0003−0338−441X], Gaspare Santaera[1,2][0009−0008−6858−4184], Paolo Dario[1,2][0000−0001−9489−0056], Cesare Stefanini[1,2][0000−0003−0989−041X], and Donato Romano[1,2][0000−0003−4975−3495]

[1] The BioRobotics Institute, Scuola Superiore Sant'Anna, Viale R. Piaggio 34, 56025 Pontedera (PI), Italy
[2] The Department of Excellence in Robotics and AI, Scuola Superiore Sant'Anna, Viale R. Piaggio 34, 56025 Pontedera (PI), Italy
{gianluca.manduca,gaspare.santaera,paolo.dario,
cesare.stefanini,donato.romano}
@santannapisa.it

Abstract. Bioinspired robots are a promising technology for minimizing environmental disruption during underwater inspection and exploration, as well as for improving animal farming conditions and protecting wildlife. In this research, we propose a control strategy for an underactuated robotic fish that mimics the oscillatory movement of a real fish's tail using only one DC motor. Our control strategy is bioinspired by Central Pattern Generators (CPGs) and integrates proprioceptive sensory feedback. Specifically, we incorporated the angular position of the tail as an input control variable to enhance the feedback loop of the CPGs. This enables the controller to adapt to changes in the tail structure, weight, or the environment in which the robotic fish swims, allowing it to change its swimming speed and steering angular speed. Our robotic fish can swim at a speed between 0.18 and 0.26 Body Length per second (BL/s), with a tail beating frequency between 1.7 and 2.3 Hz. It can also vary its steering angular speed in the range of 0.08 rad/s, resulting in a relative change in the curvature radius of 0.25 m. With modifications to the modular design, we can further improve the speed and steering performance while maintaining the developed control strategy. This research highlights the potential of bioinspired robotics to address pressing environmental challenges while improving solutions efficiency, reliability and reducing development costs.

Keywords: biorobotics · biomimetics · underwater robotics · fish robot · proprioceptive control · environmental robotics.

* This research was carried out in the framework of the EU H2020-MSCA-RISE-2018 ECOBOTICS.SEA - Bio-inspired Technologies for a Sustainable Marine Ecosystem [824043].

1 Introduction

Underwater exploration and environmental monitoring are crucial applications of robotics in the aquatic environment, as highlighted by research in [1, 2]. Drawing inspiration from the graceful and efficient movements of underwater species, researchers aim to develop robotic solutions that can navigate with agility in complex underwater areas. Moreover, the use of bioinspired robots can mitigate the disturbance to underwater ecosystems, while also potentially improving animal farming conditions, preserving wildlife, and aiding in the control of animal populations in agriculture, as discussed in [3, 4].

The rich biodiversity found underwater has inspired the design and control strategies of numerous marine robots, as highlighted in [5]. Among various locomotion strategies used in aquatic environments, carangiform and subcarangiform swimmers are capable of achieving high speeds, albeit at the cost of reduced maneuverability compared to anguilliform swimmers, which have more degrees of freedom.

Underactuated mechanisms can provide robust and reliable solutions for robotic systems. El Daou et al. [6] developed a compliant body subcarangiform robot with a linked fin, while [7] used an active wire-driven body and a passive compliant body. Zhong et al. [8] also used a wire-driven mechanism to achieve high-speed swimming, and a two-joint-centred compliant tail was employed for maneuverability in [9]. Alternatively, hydraulic actuation was utilized in the robot proposed in [10]. Moreover, magnetic actuation is rapidly gaining popularity in the field of robotics due to its simplicity, robustness, and reliability. Magnetic actuation allows for the separation of the fish tail's moving parts in contact with water from the electronic components, thereby improving waterproofing and reducing the risk of motor overload in the event that the tail cannot move. This makes magnetic actuation an ideal choice for designing underwater robots that require enhanced durability and resilience in challenging environments. Previous studies have investigated magnetic actuation for multi-link actuated [11] and underactuated [12] robots.

Bioinspiration, however, is not limited to thrust generation; control strategy can also benefit from it. Vertebrates and invertebrates manage locomotion through Central Pattern Generators (CPGs) [13, 14]. These neural networks provide feedforward rhythmic activity. The inspiration from CPGs in the control strategy of underwater robots has been proposed in several studies [15–17]. This approach is usually used to synchronise different actuators in robots. However, CPG-based control has been shown to guarantee multi-mode swimming even of underactuated solutions [18, 19]. Proprioception refers to the perception and awareness of the body's position, movement, and orientation in space, which is provided by sensory receptors located in the muscles, joints, and tendons [20, 21]. The integration of proprioceptive sense in biological systems allows for adaptive management of rhythmic activity [22, 23]. This concept has been applied to bioinspired underwater robots through the use of feedback control strategies that incorporate information from proprioceptive sensors. In the study [24], it was demonstrated by means of a robotic fish with multi-joint actuation that

fishes are able to save energy by means of proprioceptive feedback. Also [25] proposed a control strategy with proprioceptive feedback for an underactuated robotic fish.

Our research focuses on developing a novel control strategy based on proprioceptive feedback for an underactuated robotic fish inspired by pelagic fishes. The proposed robot features subcarangiform locomotion and a non-blocking actuation mechanism that generates a tail swing through the interaction of magnets and a coupling of vertebrae via a wire system, all driven by an oscillating movement of a single DC motor. In this updated version of the robot proposed in [12], we have incorporated an electronic control apparatus and changed the actuation system from a one-way motor movement to a back-and-forth solution. Moreover, in contrast to the previous version, the updated robot can not only vary its swimming speed but also its direction, thanks to the integration of a bioinspired control strategy that enhances the robot's maneuverability and allows for adaptation to different environments and loads on the tail.

2 Materials and Methods

2.1 Modelling of the Travelling Wave

The bioinspired robotic fish developed takes pelagic fishes as a biological reference, and it generates the thrust by bending its body into a propulsive wave that extends back to its caudal fin. Fig. 1 shows the artifact structure, the working principle of the actuation system, and the reference systems. The body and /or caudal fin (BCF) locomotion is typical of most fish in nature and can be described as an amplitude-modulated traveling wave [26], [27]. As proposed by [28], the following equation can model the travelling wave in the case of carangiform robotic fish:

$$y_t(x,t) = (c_1 x_t + c_2 x_t^2)\sin(kx_t - \omega t), \tag{1}$$

Equation 1 describes a body wave traveling from head to tail in a body-fixed coordinate system with the abscissa positive towards the tail. y_t and x_t are the sideward and axial displacement, respectively, in the coordinate system $\{S_t\}$ presented in Fig. 1(b), while t denotes the time. $k = 2\pi/\lambda$ is the wave number, λ represents the wavelength, and ω is the wave frequency. c_1 and c_2 are the wave amplitude's linear and quadratic coefficients, respectively. The last two parameters can be adjusted to achieve the desired BCF swimming mode. We remind to the previous work for a more comprehensive description [12].

2.2 Structure & Mechanism

The robotic platform comprises a water-resistant head and an oscillating mechanism that is exposed to water, as shown in Fig. 1(a). The head contains all the necessary electronics, while the oscillating mechanism is composed of a peduncle, three segments, two hinges, and a final caudal fin inserted into the final joint. The wire mechanism connects the three segments to the head, see Fig. 1(c). The

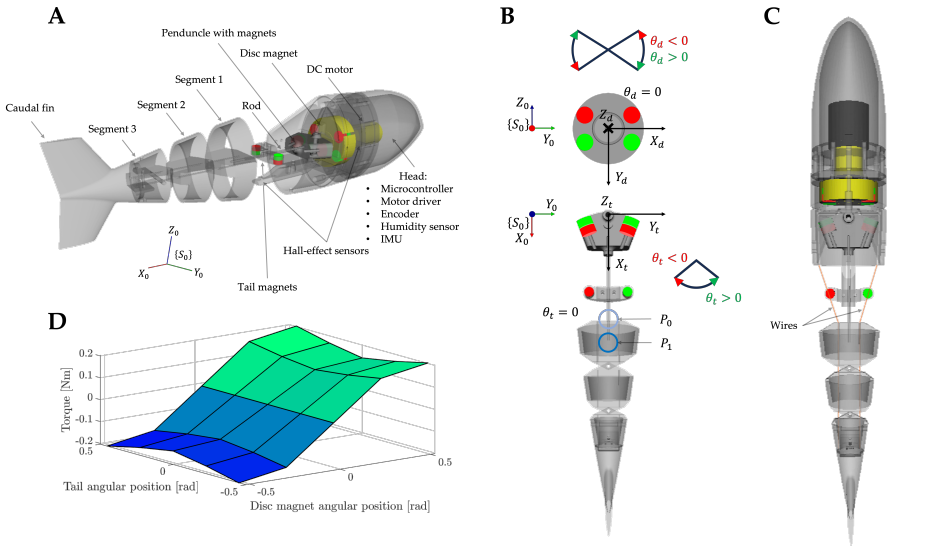

Fig. 1. Robotic fish design: (**a**) Structure representation with the related components description. (**b**) Reference coordinate systems considered. (**c**) Visual representation of the wire system. (**d**) Torque exerted on the tail by the magnetic coupling between disc magnet and oscillating arm magnets according to different disc magnet/tail configurations.

motor, located in the head, oscillates a plastic disc that contains four permanent magnets (disc magnet). The magnets' arrangement and orientation divide the disc magnet into two areas with different polarities. Two magnets on the peduncle face the disc side with the same polarity. The contactless mechanical power transmission between the disc magnet and the peduncle magnets results from the attractive/repulsive forces. There is no passive actuation, and all segments are linked by wires. When the magnets on the disc attract one of the peduncle magnets, the other is repelled, causing the oscillating rod to bend to the attracted magnets' side while the tail tip points to the repelled magnet's side. See Fig. 2 for a visual representation of the actuation mechanism. Because there is no mechanical connection between the motor shaft and the oscillating arm, the system is non-blocking and prevents the DC motor and the entire structure from overloading. If the fish tail were to become stuck, it would remain in a fixed position while the motor continued running smoothly, breaking the magnetic coupling.

The current robotic design represents an evolution of a prior prototype developed at the BioRobotics Institute of Scuola Superiore Sant'Anna (Pisa, Italy) [12], with several significant changes. While the previous version of the robot validated the non-blocking actuation system with a single DC motor and excluded any electronic components from the body, the present version increased

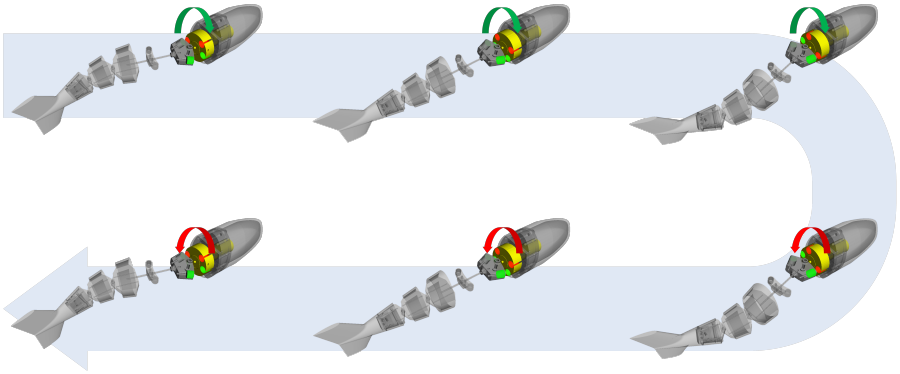

Fig. 2. Visual representation of the actuation mechanism.

the robot's size. The distance between the two ends of the body now measures 400 mm with a weight of 875 g, as opposed to the prior version that measured only 179 mm in length and weighed 77 g. The current design integrates a motor driver, a microcontroller, and a sensor apparatus that includes an optical encoder, hall-effect sensors, an inertial measurement unit (IMU), and a humidity sensor. The current design also features different magnets and a motor with back-and-forth actuation, in contrast to the previous version that used a continuous unidirectional motor rotation.

The position of the disc magnet θ_d determines the magnetic force exerted on the tail. The force values have been empirically measured with different disc magnet/tail configurations through a dynamometer placed in P_0 Fig. 1(b). Fig. 1(d) shows the results converted into torque values. When $\theta_d = 0$ rad, neutral position, the attraction/repulsive forces exerted by the disc magnet on the tail are zero. An oscillation of the disc magnet around the neutral position generates an oscillation of the tail. When $\theta_d = \pm\ 0.52$ rad, the interaction forces between disc magnet and tail are maximal.

The optical encoder in the head, coupled with the electric motor, provides the shaft's relative position, speed, and acceleration. An Hall-effect sensor, measures the magnetic field of the disc magnet, determining its absolute position during an initial setting phase. Another bipolar Hall-effect sensor measures the magnetic field of two magnets placed on the tail rod, see Fig. 1. The magnets face with different polarities on the sensor. During tail oscillation, the bipolar Hall-effect sensor thus measures an oscillation of the magnetic field. The curve relating the tail angular position and the sensor measurements has been characterized by interpolation through the Matlab software Curve Fitting Tool. Different functions have been evaluated. A second-degree polynomial had better fit the extrapolated data by considering two different sets of parameters according to the θ_t angle sign.

2.3 Control Strategy

By generating a rhythmic activity of the disc magnet, it is possible to obtain in response a tail oscillation, similar to how locomotion is handled by CPGs in vertebrates and invertebrates [13]. These central neural networks determine the appropriate set of activation of the muscles without requiring feedback from the sensors. Motion management, in this sense, resorts to a feed-forward control, thus ensuring the exact torque to achieve goal-directed motion at certain speeds [14, 29]. Since our robotic fish features a non-mechanically coupled system, a feed-forward control approach would not be suitable for various environments conditions and could be challenging to implement. This is because the oscillation frequency and amplitude would need to be calibrated taking into account the interaction forces that depend on the environment in which the robotic fish swims. Failure to accurately calibrate these parameters could cause a decoupling of the actuation system, resulting in undesired movements. Therefore, a more adaptable and effective solution is to use a feedback control approach, such as our bioinspired control strategy that incorporates proprioceptive feedback and enables the robot to adapt to different environment conditions and loads. For this reason, as also proposed in [25], oscillatory action is integrated with proprioceptive sensory feedback.

We therefore proposed a parameterised control law that receives as input the position of the tail as proprioceptive feedback. The disc magnet configuration determines the torque exerted on the fishtail which is the control action considered. The following equation expresses the proposed control low, which is composed of three contributions:

$$\tau_t(\hat{\theta}_t) = \tau_{t,1}(\hat{\theta}_t) + \tau_{t,2}(\hat{\theta}_t) + \tau_s(\hat{\theta}_t), \tag{2}$$

where

$$\tau_{t,1}(\hat{\theta}_t) = k_1 sign(\dot{\hat{\theta}}_t)(1 - |\hat{\theta}_t|), \tag{3}$$

$$\tau_{t,2}(\hat{\theta}_t) = -k_2\hat{\theta}_t, \tag{4}$$

$$\tau_s(\hat{\theta}_t) = k_s(1 - |\hat{\theta}_t|). \tag{5}$$

$\hat{\theta}_t$ is the tail angle θ_t divided by its maximum value resulting in $\hat{\theta}_t \in [-1.1]$. $\tau_{t,1}(\hat{\theta}_t)$ generates a torque contribution that varies its sign according to the direction of the tailbeat, with maximum and minimum peaks at $\hat{\theta}_t = 0$. It becomes null when the tail reaches the end strokes ($\hat{\theta}_t = \pm\, 1$). $\tau_{t,2}(\hat{\theta}_t)$ opposes $\tau_{t,1}(\hat{\theta}_t)$ to guarantee a call-back to the tail when reaching the end strokes. Unlike $\tau_{t,1}(\hat{\theta}_t)$, it has maximum and minimum peaks when $\hat{\theta}_t = \pm\, 1$ and vice versa it cancels at $\hat{\theta}_t = 0$. $\tau_s(\hat{\theta}_t)$ instead is the steering contribution. It generates an asymmetry in $\tau_{t,1}(\hat{\theta}_t)$, increasing the value towards one direction and decreasing towards the other. The control law is therefore:

$$\tau_t(\hat{\theta}_t) = (k_1 sign(\dot{\hat{\theta}}_t) + k_s)(1 - |\hat{\theta}_t|) - k_2\hat{\theta}_t, \tag{6}$$

and it is governed by three parameters k_1, k_2 and k_s. k_1 is a positive parameter.

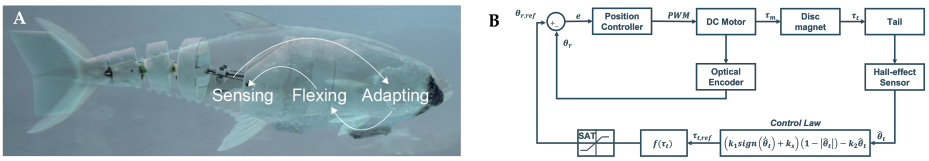

Fig. 3. General description of the bioinspired approach (**a**) and block diagram of the system (**b**).

It varies the $\tau_{t,1}(\hat{\theta}_t)$ and thus the torque exerted on the tail during the beat with a consequent increase in oscillation frequency. k_2 is also a positive parameter and determines the value of torque that the tail receives at the end-strokes to oppose the motion and change direction of the beat. k_2 must always be less than k_1, otherwise the control would impose a decrease in torque during the tail restart. The sign of k_s determines the direction of curvature. Its value, on the other hand, varies the asymmetry between one direction of tail beating and the opposite one. Since k_s diminishes the k_1 effect in one direction while augmenting it in the opposite one, it must not diminish k_1 to such an extent that it becomes less than k_2 for the same reasons explained above. The following system collects the constraints to which the three parameters are subject:

$$\begin{cases} k_1, k_2 > 0 \\ k_1 > k_2 \\ (k_1 - |k_s|) > k_2. \end{cases} \tag{7}$$

We approximated the relation between the torque exerted on the fishtail and the disc magnet angular position with the following linear function:

$$\theta_d = k_{ln}\tau_t(\hat{\theta}_t). \tag{8}$$

θ_d is the angular position of the disc magnet (rad) according to the coordinate system $\{S_t\}$ in Fig. 1(b). k_{ln} is a parameter that converts the desired torque into the disc magnet position, and it is related to the angular operating region of the disc magnet and the maximum torque allowed by the system. If the normalised torque value is considered, the control law can be generalised. At this point, the choice of k_{ln} depends solely on the maximum oscillation range of the disc magnet. This parameter is structural and depends on the spacing of the magnets. Therefore k_{ln} must equal this value, which, as mentioned in the previous subsection, corresponds to 0.52. At a maximum torque value ($\tau_t(\hat{\theta}_t) = 1$), the position of the disc magnet will therefore correspond to $\theta_d = 0.52$ rad. Conversely, at a minimum torque value ($\tau_t(\hat{\theta}_t) =$ -1), θ_d will equal -0.52 rad. The overall strategy reduces to position control of the disc magnet. The reference position tracking relies on a PID controller. A Pulse Width Modulation (PWM) strategy is adopted. Fig. 3(b) shows the block scheme of the entire system. The saturation is considered to prevent the disc magnet from going beyond its operating range and nullifying the control strategy.

2.4 Experimental Set-up & Performance Assessment

The control strategy was validated by conducting experiments on the robot both in air and underwater. Initially, the robot was tested in air, where its body was held in place while allowing its tail to swing freely. Subsequently, the robot was placed in a tank measuring 1m in length and 0.5 m in height, and then in a pool measuring 10x5 m and 0.8 m in depth. A camera with a 12 MP resolution and f/2.2 aperture was used to record the predetermined trajectories (rectilinear and circular), and the distances traveled were extrapolated using post-processing analysis. Travel times of a predefined stretch were collected to determine the speed, and data on the position of the disc magnet and tail were saved in the robot's internal memory for later analysis. The controller's adaptability to different conditions and the possibility of varying swimming performance in relation to the control law's parameters were evaluated to assess the results.

3 Experimental Results

The PID controller was tuned using the Ziegler-Nichols method ($k_p = 0.15$, $k_d = 0.1$, and $k_i = 0$). Fig. 4(a) shows the tail beating oscillation in relation with the disc magnet one for a given set of parameters ($k_1 = 1$, $k_2 = 0.4$, $k_s = 0$) considering the fish robot stuck in water. Just as defined by the control law, the maximum and minimum values of the angular position of the disc magnet correspond to the moment when the position of the tail is close to zero. The contribution of non-zero k_2, allows the disc magnet, not to be in the neutral position when the tail reaches the end of the stroke. The call-back contribution thus generated, allows the tail not to stall and generate a continuous oscillation. With the same parameters, Fig. 4(b) presents the change in tail frequency according to different environmental and load conditions. Frequencies were obtained with *plomb* Matlab function by considering the maximum peak of the periodigram. The results compare the control considering the robot first in air and then in water. In the latter case, two different weights (75 and 140 g) were then added to the first tail segment, 0.1 m from its axis of rotation. Without the integration of proprioceptive feedback, the frequency would have remained the same for all cases considered. The amplitude of oscillation of the tail would decrease as the load on the tail increases. The control would therefore lose the coupling between the disc magnet and the tail. A feed-forward solution would require a calibration of parameters for each presented condition. The strategy developed in this work results instead adaptive to changes in shape, the weight of the tail, or liquid density in which the robotic fish swims, thanks to proprioceptive feedback.

Instead, a change in controller parameters generates a change in swimming performance as presented in Fig. 5. In the following, the swimming speed of the robot will be indicated in Body Length per second (BL/s). Varying k_1 and maintaining the remaining parameters fixed, as discussed in the previous section, we expect a change in the tail beating frequency reflecting on a change in the swimming speed. Fig. 5(a) shows the velocity value of the robotic fish and the corresponding value of the tailbeat frequency, as k_1 changes, with k_s

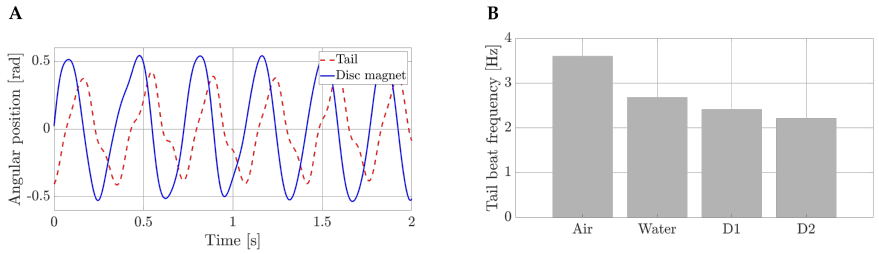

Fig. 4. Control strategy validation in nominal condition ($k_1 = 1$, $k_2 = 0.4$, and $k_s = 0$) with the robotic fish stuck: (**a**) Phase shift between the angular position of the tail and the disc magnet (test in water). (**b**) Tail beat change in frequency according to different environments (air - water) and different loads applied to the tail (D1 = 75 g, D2 = 140 g, water tests).

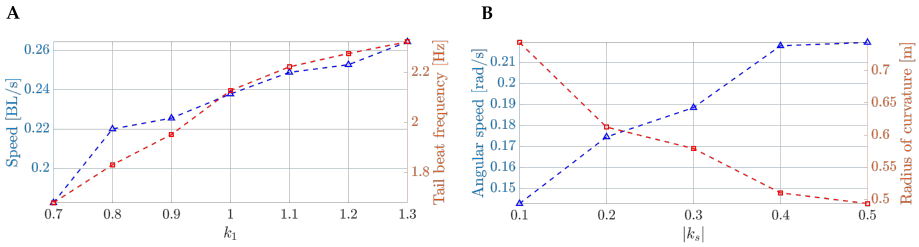

Fig. 5. Robotic fish performances according to the control parameters choice: (**a**) Change in tail beat frequency (red line) and the related robotic fish body speed (blue line) considering different values of k_1 with $k_2 = 0.4$, and $k_s = 0$, fixed. (**b**) Angular radius (red line) and speed (blue line) varying the steering parameter k_s with $k_1 = 1$, and $k_2 = 0.4$, fixed.

$= 0$ and $k_2 = 0.4$ fixed. Results prove the hypothesis assumed. The tail beating frequency varies between ~ 1.7 Hz and ~ 2.3 Hz. The measured swimming speed values change with the same trend between ~ 0.18 BL/s and ~ 0.26 BL/s. Subsequently, the possibility of changing curvature direction and performance was investigated. Fig. 5(b) shows the steering performance in terms of angular velocity and angle of curvature as k_s varies, keeping $k_1 = 1$, and $k_2 = 0.4$. The robotic fish can vary the steering angular speed in the range of ~ 0.08 rad/s with a relative change in the curvature radius of 0.25 m. Fig. 6 presents a visual representation of the experimental results, showcasing the abilities of the developed control strategy. The trajectory of the robotic fish follows a circular path, demonstrating the effectiveness of the control parameters chosen to guide the fish's movement. Considering the curves empirically obtained, the robotic fish developed, according to the bioinspired control strategy proposed, shows a range of maneuverability despite its underactuated design.

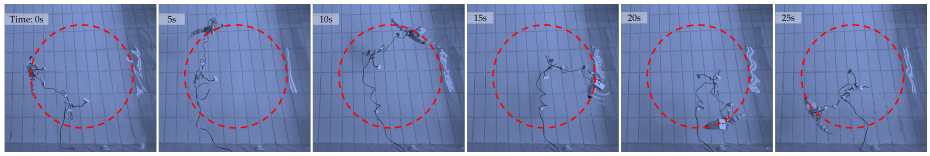

Fig. 6. Swimming pool experiments: Image sequence (25 s) of the swimming fish robot with the parameters $k_1 = 1$, $k_2 = 0.4$, and $k_s = -0.5$.

4 Discussion

This study presents a novel bioinspired control approach for an underactuated robotic fish. While a previous work [12] validated the actuation system, the initial version of the robot lacked an electronic system and did not explore any control strategies.

The control strategy proposed in this study manages the rhythmic movement of the robotic fish's tail in a manner similar to that of CPGs. Previous literature has utilized CPGs to coordinate numerous actuators for oscillatory movements [15–17]. In another investigation, a lamprey-like robotic fish was reproduced using a similar implementation system to the one proposed here. However, the system in that study was not underactuated and comprised active and passive vertebrae to produce an anguilliform locomotion [11]. Xie et al. [18] have shown that a CPG-based control can ensure multimodal swimming of an underactuated system. However, they used a wire-driven mechanism and did not consider magnetic actuation.

The real novelty, however, of our proposed work lies in the integration of proprioception for the motor management of the robotic fish. In the study carried out by Li et al. [24], it was demonstrated by means of a robotic fish with multi-joint actuation that fishes are able to save energy by means of proprioceptive feedback. The researchers considered a CPG controller that adjusts the body undulation of the robot after receiving feedback from the proprioceptive sensing signal. They considered the force or force-related signals as the proprioceptive signal from the caudal fin, decoded via reinforcement learning. Sánchez-Rodríguez et al. [25] integrated the information from the proprioceptive sensors to moderate the tail deformation in an underactuated solution. An actuation based on mechanical coupling and a force sensor was considered. In contrast, we proposed this approach on a non-blocking type of actuation, considering the tail position information as proprioceptive feedback. This solution, through the proposed parameterised control law, is thus able to adapt the rhythmic activity of the tail according to the environment in which the robotic fish swims and the load supported. Furthermore, the variation of control law parameters enables the robot's manoeuvrability. This study opens the door to an integration of exteroceptive sensors for autonomous swimming.

The robot proposed in this work, in accordance with the control strategy developed, proved to be able to vary the swimming speed by 0.08 BL/s reaching

a maximum speed of 0.26 BL/s with a relative tail-beat frequency of 2.3 Hz. The swimming performance has clear margins for improvement when compared with other works, such as [7] in which speeds of 2.02 BL/s at a tail-beat frequency of 5.46 Hz are achieved. In fact, the intention of the work was to propose and validate a control strategy that would make a previously proposed implementation system effective. The work was therefore not focused on swimming performance. In comparison with the previous version, the speed decreased by 0.47 BL/s. However, several factors must be considered in the comparison. Firstly, the reduced size of the first version of the robot, which weigthed 77 g compared to the 875 g of the one proposed in this work, having a larger volume for the insertion of electronic components. Secondly, the maximum tailbeat frequency reached by the first version was higher (3.25 Hz). This aspect is related to the sizing of the magnets. By introducing magnets with a higher attractive/repulsive force, better performance can be achieved. Furthermore, the modular design allows performance improvements to be investigated secondarily. Different designs can be integrated and compared while maintaining the same control strategy.

The successful steering of the robot was achieved by utilizing an asymmetric tail-beat, which was inspired by natural behavior [30, 31]. Meurer et al. [32] also employed a similar mechanism in a compliant robotic fish using a nonlinear controller, but with a mechanically coupled actuation system and without considering proprioception. On the other hand, classical approaches for steady turning maneuvers involve changing the center of oscillation of the robot's tail, which require large tail deflections to be effective [33, 34]. However, the robot presented in this study has relatively small tail segments with space in between them. The results showed a change in angular velocity of 0.08 rad/s with a respective change in curvature angle of 0.25 m. To improve these results, a larger lateral tail surface and reducing the spaces between the vertebrae could be considered. Future studies could also involve incorporating a strategy based on changing the center of oscillation of the tail for comparison.

The control strategy developed in this work manages the rhythmic activity of the robotic fish's tail in a way that resembles how CPGs control the activation of muscles. This allows the strategy to adapt to changes in the tail's structure, weight, or environment through proprioceptive feedback. The system's speed and steering performances could be improved by making design changes to the modular structure while maintaining the control strategy. The underactuated solution provides the benefits of increased reliability and energy savings. Future investigations will focus on evaluating the energy consumption of the proposed platform, exploring different approaches to swimming deeper, and integrating exteroceptive sensors like cameras to enable autonomous swimming. This robotic platform could be used for non-invasive environmental monitoring operations and animal/robot interactions within the marine ecosystem.

Acknowledgements The authors are grateful to the communal swimming pool of Pontedera staff for having made available their own spaces to do the experiments. The authors also thank Dr. Gloria Bianco and Mr. Raffaele Picichè for

their assistance during the tests and their graphic support and Mr. Godfried Jansen Van Vuuren and Dr. Marco Miraglia for their technical support during the design and development of the robotic artifact.

References

1. Mayer, L., Jakobsson, M., Allen, G., Dorschel, B., Falconer, R., Ferrini, V., ... Weatherall, P. (2018). The Nippon Foundation—GEBCO seabed 2030 project: The quest to see the world's oceans completely mapped by 2030. Geosciences, 8(2), 63.
2. Halpern, B. S., Frazier, M., Afflerbach, J., Lowndes, J. S., Micheli, F., O'Hara, C., ... Selkoe, K. A. (2019). Recent pace of change in human impact on the world's ocean. Scientific reports, 9(1), 1-8.
3. Ryuh, Y. S., Yang, G. H., Liu, J., Hu, H. (2015). A school of robotic fish for mariculture monitoring in the sea coast. Journal of Bionic Engineering, 12(1), 37-46.
4. Kruusmaa, M., Gkliva, R., Tuhtan, J. A., Tuvikene, A., Alfredsen, J. A. (2020). Salmon behavioural response to robots in an aquaculture sea cage. Royal Society open science, 7(3), 191220.
5. Li, Y., Xu, Y., Wu, Z., Ma, L., Guo, M., Li, Z., Li, Y. (2022). A comprehensive review on fish-inspired robots. International Journal of Advanced Robotic Systems, 19(3), 17298806221103707.
6. El Daou, H., Salumäe, T., Toming, G., Kruusmaa, M. (2012, May). A bio-inspired compliant robotic fish: Design and experiments. In 2012 IEEE International Conference on Robotics and Automation (pp. 5340-5345). IEEE.
7. Van Den Berg, S. C., Scharff, R. B., Rusák, Z., Wu, J. (2020). Biomimetic design of a soft robotic fish for high speed locomotion. In Biomimetic and Biohybrid Systems: 9th International Conference, Living Machines 2020, Freiburg, Germany, July 28–30, 2020, Proceedings 9 (pp. 366-377). Springer International Publishing.
8. Zhong, Y., Li, Z., Du, R. (2017). A novel robot fish with wire-driven active body and compliant tail. IEEE/ASME Transactions on Mechatronics, 22(4), 1633-1643.
9. Yu, J., Zhang, C., Liu, L. (2016). Design and control of a single-motor-actuated robotic fish capable of fast swimming and maneuverability. IEEE/ASME Transactions on Mechatronics, 21(3), 1711-1719.
10. Katzschmann, R. K., Marchese, A. D., Rus, D. (2015, November). Hydraulic autonomous soft robotic fish for 3D swimming. In Experimental Robotics: The 14th International Symposium on Experimental Robotics (pp. 405-420). Cham: Springer International Publishing.
11. Stefanini, C., Orlandi, G., Menciassi, A., Ravier, Y., La Spina, G., Grillner, S., Dario, P. (2006, February). A mechanism for biomimetic actuation in lamprey-like robots. In The First IEEE/RAS-EMBS International Conference on Biomedical Robotics and Biomechatronics, 2006. BioRob 2006. (pp. 579-584). IEEE.
12. Romano, D., Wahi, A., Miraglia, M., Stefanini, C. (2022). Development of a Novel Underactuated Robotic Fish with Magnetic Transmission System. Machines, 10(9), 755.
13. Grillner, S. (2003). The motor infrastructure: from ion channels to neuronal networks. Nature Reviews Neuroscience, 4(7), 573-586.
14. Grillner, S. (2006). Biological pattern generation: the cellular and computational logic of networks in motion. Neuron, 52(5), 751-766.

15. Zhao, W., Hu, Y., Zhang, L., Wang, L. (2009). Design and CPG-based control of biomimetic robotic fish. IET control theory applications, 3(3), 281-293.
16. Stefanini, C., Orofino, S., Manfredi, L., Mintchev, S., Marrazza, S., Assaf, T., ... Dario, P. (2012). A novel autonomous, bioinspired swimming robot developed by neuroscientists and bioengineers. Bioinspiration biomimetics, 7(2), 025001.
17. Thandiackal, R., Melo, K., Paez, L., Herault, J., Kano, T., Akiyama, K., ... Ijspeert, A. J. (2021). Emergence of robust self-organized undulatory swimming based on local hydrodynamic force sensing. Science Robotics, 6(57), eabf6354.
18. Xie, F., Zhong, Y., Du, R., Li, Z. (2019). Central pattern generator (CPG) control of a biomimetic robot fish for multimodal swimming. Journal of Bionic Engineering, 16, 222-234.
19. Chen, J., Yin, B., Wang, C., Xie, F., Du, R., Zhong, Y. (2021). Bioinspired closed-loop CPG-based control of a robot fish for obstacle avoidance and direction tracking. Journal of Bionic Engineering, 18, 171-183.
20. Tuthill, J. C., Azim, E. (2018). Proprioception. Current Biology, 28(5), R194-R203.
21. Laskowski, E. R., Newcomer-Aney, K., Smith, J. (2000). Proprioception. Physical medicine and rehabilitation clinics of North America, 11(2), 323-340.
22. Pearson, K. G. (1995). Proprioceptive regulation of locomotion. Current opinion in neurobiology, 5(6), 786-791.
23. Ryczko, D., Simon, A., Ijspeert, A. J. (2020). Walking with salamanders: from molecules to biorobotics. Trends in neurosciences, 43(11), 916-930.
24. Li, L., Liu, D., Deng, J., Lutz, M. J., Xie, G. (2021). Fish can save energy via proprioceptive sensing. Bioinspiration biomimetics, 16(5), 056013.
25. Sánchez-Rodríguez, J., Celestini, F., Raufaste, C., Argentina, M. (2021). Proprioceptive mechanism for bioinspired fish swimming. Physical Review Letters, 126(23), 234501.
26. Sfakiotakis, M., Lane, D. M., Davies, J. B. C. (1999). Review of fish swimming modes for aquatic locomotion. IEEE Journal of oceanic engineering, 24(2), 237-252.
27. Blake, R. W. (2004). Fish functional design and swimming performance. Journal of fish biology, 65(5), 1193-1222.
28. Barrett, D. S., Triantafyllou, M. S., Yue, D. K. P., Grosenbaugh, M. A., Wolfgang, M. (1999). Drag reduction in fish-like locomotion. Journal of Fluid Mechanics, 392, 183-212.
29. Yu, J., Tan, M., Chen, J., Zhang, J. (2013). A survey on CPG-inspired control models and system implementation. IEEE transactions on neural networks and learning systems, 25(3), 441-456.
30. Gray, J. (1933). Directional control of fish movement. Proceedings of the Royal Society of London. Series B, Containing Papers of a Biological Character, 113(781), 115-125.
31. Webb, P. W., Fairchild, A. G. (2001). Performance and maneuverability of three species of teleostean fishes. Canadian Journal of Zoology, 79(10), 1866-1877.
32. Meurer, C., Simha, A., Kotta, Ü., Kruusmaa, M. (2019, May). Nonlinear orientation controller for a compliant robotic fish based on asymmetric actuation. In 2019 International Conference on Robotics and Automation (ICRA) (pp. 4688-4694). IEEE.
33. Hu, Q., Hedgepeth, D. R., Xu, L., Tan, X. (2009, May). A framework for modeling steady turning of robotic fish. In 2009 IEEE International Conference on Robotics and Automation (pp. 2669-2674). IEEE.
34. Tan, X., Carpenter, M., Thon, J., Alequin-Ramos, F. (2010, May). Analytical modeling and experimental studies of robotic fish turning. In 2010 IEEE International Conference on Robotics and Automation (pp. 102-108). IEEE.